Optimized ultrasonic attenuation measures for non-homogeneous materials

V. Genovés[a,*], J. Gosálbez[b,**], A. Carrión[b], R. Miralles[b], J. Payá[a]

[a] *ICITECH, Universitat Politècnica de València, Camino de Vera, s/n 46022 Valencia, Spain*
[b] *ITEAM, Universitat Politècnica de València, Camino de Vera, s/n 46022 Valencia, Spain*

Abstract

In this paper the study of frequency-dependent ultrasonic attenuation in strongly heterogeneous materials was addressed. To determine the attenuation accurately over a wide frequency range, it is necessary to have suitable excitation techniques. In this study, three kinds of transmitted signals have been analyzed, grouped according to their bandwidth: narrowband and broadband signals. Its mathematical formulation has revealed the relationship between the distribution of energy in their spectra and its immunity to noise. Sinusoidal and burst signals present higher signal-to-noise ratio (SNR) but a large number of measurements to cover the frequency range is needed. However, the linear swept-frequency signals (chirp) at the expense of lower SNR improve the effective bandwidth covering a wide frequency range with a single measurement and equivalent accuracy. In the case of highly attenuating materials, it is proposed the use of different configurations of the chirp signals which enable to inject more energy, and therefore, to improve the sensitivity of the technique without involving a high time cost. So that, if the attenuation of material and the sensitivity of measurements equipment allow the use of broadband signals, the combination of this kind of signals and the suitable signal processing result in an optimal estimate of frequency-dependent attenuation with a minimum measurement time.

Keywords:
Chirp signal, Attenuation, Concrete, Ultrasonics, Frequency sweep

Contents

*Corresponding author E-mail adress: genoves.gomez@gmail.com
**Corresponding author E-mail adress: jorgocas@dcom.upv.es

1. Introduction

Concrete is a non-homogeneous material prepared by mixing cement, aggregates and water used mainly in the field of civil and building engineering [1]. Due to its non-homogeneous structure, this material in its hardened state is composed by air voids, interfaces between aggregates and hydrated cement paste, micro-cracks and other defects inside its microstructure. For that reason, concrete is a very dispersive material and hard to measure (in order to know its physical and mechanical conditions) indirectly with non destructive techniques (NDT) [2].

Several authors tried to test cement-based materials using different NDT in order to characterize concrete properties and detecting damage by means of monitoring diverse parameters [3–5].

Due to its robustness, one of the most widely used parameters for ultrasonic NDT is the ultrasonic pulse velocity. However, the attenuation is considered a more sensitive parameter to structural properties of the material. Taking into account that is a parameter related to the energy of the wave, is more affected than ultrasonic velocity to experimental setup such as coupling problems between ultrasonic sensors and analysed material, energy loss due to wires, connectors, devices, etc [6–9]. Despite of these problems, the determination of the frequency-dependent ultrasonic attenuation, $\alpha(f)$, [6, 8, 10–12], is a useful parameter due to its sensitivity to many defects on materials (voids, cracks...) and properties, specifically on concrete where the water to cement ratio and cement to aggregate ratio are important variables on concrete design and they determine its mechanical and physical properties.

Several authors have used different techniques to measure the attenuation on cementitious materials. The typical setup is a through-transmission where the transmission transducer is excited with an electrical signal to generate the ultrasonic signal. The transmitted signals can be narrowband ([8, 13–15]) and broadband signals ([6, 8, 16]). On one hand, narrowband signals provide good performance against high attenuating materials, due to its high signal to noise ratio (SNR), but they require a large number of measurements to estimate the $\alpha(f)$ curve (one measure per each point of the curve). On the other hand, the broadband signals require much less measurements because they cover a wider frequency range, but are more affected by noise because its energy is distributed over a wider frequency range.

Using broadband signals implies several advantages. Beyond practical ones (time cost), there exist real applications which cannot be correctly monitorized due to the fact that the system under study fastly varies along

the time. In that situations, it is needed the use of a configuration which allows to measure attenuation efficiently without losing accuracy. The aims of this paper are to analyze each kind of transmitted signal, to provide an optimal method to obtain the frequency-dependent attenuation, $\alpha(f)$, and to compare the attenuation results achieved by each configuration on a particular real application: measuring Portland cement mortar specimens.

The remainder of this work is structured as follows. Section 2 describes and mathematically formulates the analysis of two narrowband signals (sinusoidal and burst signals) and a broadband signal (chirp signal), as well as the theoretical and experimental expressions for $\alpha(f)$ in each case. Different configurations for the chirp signal are analysed in order to evaluate its noise immunity. In Section 3 the experiment which validates the aforementioned expressions is explained: materials and test layout. Section 4 presents the achieved attenuation results and, finally, conclusions are summarized.

2. Mathematical background

In a through-transmission inspection, the energy spectral density (ESD)[1] of the received signal (in frequency domain), $S_{rx}(f)\,[dB]$, can be modeled as Eq. (1):

$$S_{rx}(f) = S_{tx}(f) - \alpha_{mat}(f) \cdot d_{mat} - \alpha_{equip}(f) \tag{1}$$

where $S_{tx}(f)\,[dB]$ is the ESD of the transmitted signal, $\alpha_{mat}\,[dB/cm]$ is the attenuation produced by the specimen, $d_{mat}\,[cm]$ is the distance between both transducers and $\alpha_{equip}(f)\,[dB]$ is the attenuation of the measurement equipment (amplifier, wires and frequency response of the emitter and receiver transducers).

From Eq. 1, the attenuation of the material, $\alpha_{mat}(f)[dB/cm]$, can be obtained in terms of the rest of variables resulting Eq. 2:

$$\alpha_{mat}(f) = \frac{10log\,(S_{tx}(f)) - 10log\,(S_{rx}(f)) - \alpha_{equip}(f)[dB]}{d_{mat}} \tag{2}$$

The challenge of this work lies in the estimation of either $S(f)$, which relates the transmitted energy/power and received energy/power as function of frequency. The following aspects must be taken into account.
The signal to noise ratio (SNR) is directly proportional to the sensitivity of the attenuation parameter. Therefore, the kind of the transmitted signal and its energy distribution in the frequency domain will condition the accuracy of the method. Working with sinusoidal or burst signals, the energy will be focused on a narrowband (higher SNR), but the estimation of $\alpha_{mat}(f)$ will correspond only to that narrow bandwidth. Consequently, in order to cover a wide spectrum it is required to employ a higher number of input signals varying its fundamental frequency (f_0). On the other hand, in the case of the chirp signal, the energy will be distributed along a wider band (lower SNR) and the estimation of $\alpha_{mat}(f)$ covers a higher range of frequencies with a single input signal. It must be

[1] The energy spectral density, $S(f)$, of a finite time signal, $x(t)$, is defined as $S(f) = |X(f)|^2$, where $X(f) = \int_{t_0}^{t_1} x(t)e^{-j2\pi f t}dt$ is the Fourier Transform of signal $x(t)$.

noticed that highly attenuation materials ($\alpha_{mat}(f)$) could required the use of signals with high density energy to be well-characterized. In Fig. 1, the temporal and frequency domains of the three types of signals are shown. It can be easily appreciated how the density of energy of sinusoidal and burst signals is higher than chirp signal one.

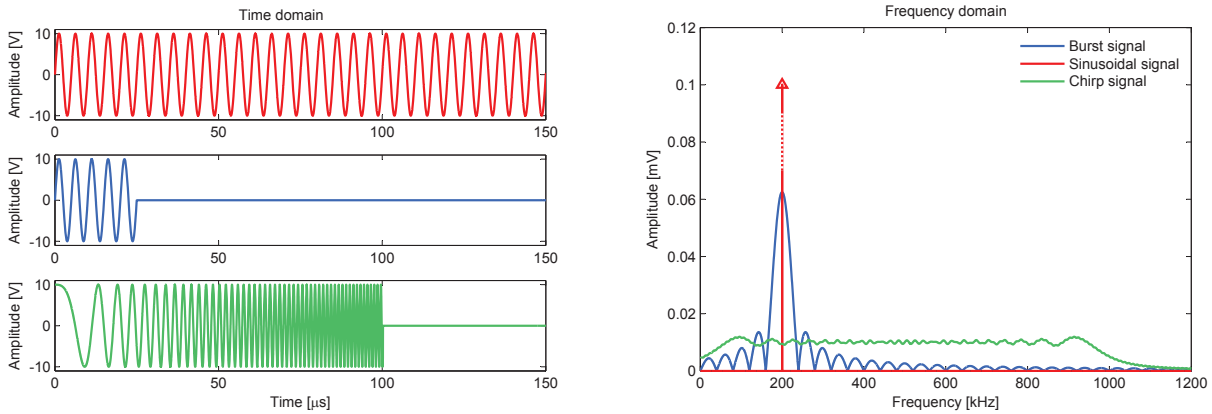

Figure 1: Comparison between narrow band signals (sinusoidal and burst) and broadband signals (chirp) in the temporal domain (left column) and frequency domain (right column). Red line corresponds to a sinusoidal signal at 200 kHz, blue line is a burst signal of 5 cycles at 200 kHz, and green line represents a chirp signal sweeping a frequency range from 100 to 900 kHz in 100 μs.

The frequency response of the equipment and, mainly, of the transducers, $\alpha_{equip}(f)$, limits the bandwidth that they are able to manage. Usually, the best performance is obtained at the fundamental frequency of transducer but it is also possible to work on the pass-band taking into account the required calibration process. The choice of the fundamental frequency depends on the material under inspection.

In this work, the aforementioned transmitted signals are analysed and proposed to evaluate the attenuation of the material, $\alpha_{mat}(f)$, in order to compare the accuracy and time cost among them. To obtain $\alpha_{mat}(f)$ it will be necessary to estimated the power/energy of the transmitted and received signals as well as the attenuation introduced by the equipment. The power/energy of the transmitted signal will be computed from its well-known theoretical expressions. However, the power/energy of the received signal will be estimated from the real acquired signals digitalized by the oscilloscope. The attenuation of equipment will be obtained by a calibration process described in Section 3.3.

2.1. Sinusoidal signal

The theoretical model of a transmitted pure sinusoidal signal is shown in Eq. 3:

$$s_{tx}(t) = A_{tx} cos\,(2\pi f_0 t + \phi_{tx}) \tag{3}$$

where A_{tx} is the amplitude of signal, f_0 is the fundamental frequency, and ϕ_{tx} is the phase of the signal that will be assumed null. An example of this signal is shown in Fig. 1 where the selected parameters for this example were: $A_{tx} = 10$ and $f_0 = 200\ kHz$. It is accepted that this signal is periodic, and therefore, it has an infinite time duration.

The theoretical spectrum of this signal (Eq. 4) presents the power focused on a single frequency, shown in Fig. 1. The power of this signal (P_{tx}) can be estimated directly from its amplitude, A_{tx} (Eq. 5). It has been assumed that the propagation medium, equipment and transducers behaves linearly. This implies that any new frequencies components will not be generated, and the received signal will be the same input signal but with different amplitude and phase which will depend only on the behaviour of the material and equipment. So that, the power of the received signal can be estimated from the amplitude of the received sinusoidal signal, $A_{rx}^{(f_0)}$ (Eq. 6).

$$S_{tx}(f) = \left| \frac{A_{tx}}{2} \left(\delta(f - f_0) + \delta(f + f_0)\right) \right|^2 \tag{4}$$

$$P_{tx} = \frac{A_{tx}^2}{2} = \frac{\max\{s_{tx}^2(t)\}}{2} \tag{5}$$

$$s_{rx}(t) = A_{rx}^{(f_0)} cos\left(2\pi f_0 t + \phi_{rx}^{(f_0)}\right) \rightarrow P_{rx}^{(f_0)} = \frac{\left(A_{rx}^{(f_0)}\right)^2}{2} \tag{6}$$

Hence, the attenuation of material for the input frequency, $\alpha_{mat}(f_0)$, can be calculated combining Eq. 5 and Eq. 6, resulting in Eq. 7:

$$\begin{aligned} \alpha_{mat}(f_0) &= \frac{P_{tx}[dB] - P_{rx}^{(f_0)}[dB] - \alpha_{equip}(f_0)[dB]}{d_{mat}} \\ &= \frac{10log_{10}\left(\frac{A_{tx}^2}{2}\right) - 10log_{10}\left(\frac{\left(A_{rx}^{(f_0)}\right)^2}{2}\right) - \alpha_{equip}(f_0)[dB]}{d_{mat}} \end{aligned} \tag{7}$$

In order to obtain the values of the $\alpha_{mat}(f_0)$ curve, it is required to do a sweep of the input fundamental frequency (f_0). The described calculations must be repeated as many times as the number of points which conform $\alpha_{mat}(f_0)$ curve. The main advantage of sinusoidal signals is its high SNR, which allows working properly on highly attenuating materials.

2.2. Burst signal

The burst signal is a common configuration used in NDT applications since it allows to estimate simultaneously several ultrasonic parameters (attenuation, velocity, etc). Its theoretical expression is a time-limited sinusoidal signal (Eq. 8):

$$s_{tx}(t) = A_{tx} \cdot cos\left(2\pi f_0 t\right) \cdot rect\left(\frac{t - \frac{NT_0}{2}}{NT_0}\right) \tag{8}$$

where A_{tx} is the amplitude of signal, f_0 is the fundamental frequency, $T_0 = \frac{1}{f_0}$ is the fundamental period of the signal, N is the number of the cycles of the signal, and $rect(\cdot)$ is the rectangular function. An example of this signal is shown in Fig. 1 where the selected parameters were: $A_{tx} = 10$, $f_0 = 200\ kHz$ and $N = 5$.

The total energy of a burst signal (Eq. (9)) depends on its fundamental frequency, f_0, the amplitude, A_{tx} and the number of cycles, N, but its theoretical spectrum (Eq. 10) represented in Fig. 1 shows that this energy is distributed in a bandwidth around the aforementioned fundamental frequency. For this reason, the energy of the transmitted and received signals must be calculated from the spectrum over a bandwidth following Eq. 11 [17]. The selected bandwidth corresponds to the main lobe of the transmitted spectrum, $f_0 \pm \frac{f_0}{N}$, and the theoretical expression for the transmitted energy over this bandwidth is Eq. 12. This energy, $E^{(f_0)}_{tx,BW}$, also depends on f_0 and represent a constant ratio of 90% of the total transmitted energy.

$$E^{(f_0)}_{tx} = \frac{A^2_{tx}}{2} N T_0 = \frac{A^2_{tx}}{2 f_0} N \tag{9}$$

$$S_{tx}(f) = \left| \frac{A_{tx} N T_0}{2} sinc\left((f - f_0) N T_0\right) e^{-j2\pi (f - f_0) N T_0} \right|^2 \tag{10}$$

$$E^{(f_0)}_{tx|rx,BW} = 2 \int_{<BW>} S_{tx|rx}(f) df = 2 \int_{f_0 - \frac{f_0}{N}}^{f_0 + \frac{f_0}{N}} S_{tx|rx}(f) df \ [J] \tag{11}$$

$$E^{(f_0)}_{tx,BW} = A^2_{tx} N \frac{1}{f_0} \frac{Si(2\pi)}{\pi} \ [J] \tag{12}$$

where $Si(\cdot)$ is the sine integral function. Using the theoretical transmitted energy (Eq. 12), and the received energy (Eq. 11), the expression of the attenuation for the corresponding input fundamental frequency, $\alpha_{mat}(f_0)$, becomes into Eq. 13:

$$\begin{aligned} \alpha_{mat}(f_0) &= \frac{E^{(f_0)}_{tx,BW}[dB] - E^{(f_0)}_{rx,BW}[dB] - \alpha_{equip}(f_0)[dB]}{d_{mat}} \\ &= \frac{10log\left(A^2_{tx} N \frac{1}{f_0} \frac{Si(2\pi)}{\pi}\right) - 10log\left(2 \int_{f_0 - \frac{f_0}{N}}^{f_0 + \frac{f_0}{N}} S_{rx}(f) df\right) - \alpha_{equip}(f_0)[dB]}{d_{mat}} \end{aligned} \tag{13}$$

Each signal has associated a fundamental frequency, f_0, so that, each measurement will evaluate just a point of the curve, $\alpha_{mat}(f)$. This implies that a frequency sweep of the fundamental frequency, f_0, has to be implemented to obtain the curve $\alpha_{mat}(f)$ evaluated in the whole defined interval. It means to take, at least, one temporal measurement for each frequency, thereby, restricting the number of analysed frequencies due to the increase of the measurement time.

2.3. Chirp signal

Swept-frequency signals (chirp) are broadband signals which enable the estimation of the curve $\alpha_{mat}(f)$ with a single measure. The mathematical expression of a linear chirp signal is showed in Eq. 14:

$$s_{tx}(t) = A_{tx} cos\left(2\pi f_0 t + \pi \Delta_{f_{max}} t^2\right) rect\left(\frac{t - \frac{T}{2}}{T}\right) \tag{14}$$

$$\Delta_{f_{max}} = \frac{f_{max} - f_0}{T} \tag{15}$$

where A_{tx} is the amplitude of the signal, f_0 is the fundamental frequency, T is the active time of the signal and $\Delta_{f_{max}}$ controls the maximum frequency ($f_{max} = f_0 + T\Delta_{f_{max}}$) which is reached at T seconds (Eq. 15). An example of this signal is shown in Fig. 1 where the selected parameters were: $A_{tx} = 10$, $f_0 = 10kHz$, $f_{max} = 1MHz$ and $T = 100\mu s$.

The mathematical expression of the spectrum of a chirp signal is more complex than the aforementioned analysed spectrums (Eq. 16)[2], but it allows to estimate $\alpha_{mat}(f)$ applying Eq. 2 directly.

$$\begin{aligned} S_{tx}(f) = \Bigg| \frac{A_{tx}}{\sqrt{2\Delta_{f_{max}}}} e^{-j\pi(f-f_0)^2} \Bigg[C\left(\sqrt{2}\frac{f-f_0}{\sqrt{\Delta_{f_{max}}}}\right) + jS\left(\sqrt{2}\frac{f-f_0}{\sqrt{\Delta_{f_{max}}}}\right) \\ - C\left(\sqrt{2}\frac{\Delta_{f_{max}}T + f - f_0}{\sqrt{\Delta_{f_{max}}}}\right) - jS\left(\sqrt{2}\frac{\Delta_{f_{max}}T + f - f_0}{\sqrt{\Delta_{f_{max}}}}\right) \Bigg] \Bigg|^2 \end{aligned} \tag{16}$$

As shown in Fig. 1, the spectrum of the transmitted pulse is distributed along a frequency bandwidth. At the expense of decreasing the SNR, broadband signals excite several frequencies simultaneously. A single acquisition allows computing $\alpha_{mat}(f)$ curve from the theoretical transmitted and received spectra. Additionally, a pseudo continuous attenuation curve is obtained instead of a discretization of $\alpha_{mat}(f)$.

Taking into account that the energy is distributed over the bandwidth of the chirp signal, the original chirp signal which swepts from 10 KHz to 1MHz has been split up into smaller frequency intervals. The division can be done in two different ways: keeping constant the energy in each interval (Mode 1) or keeping constant the total energy (Mode 2). This analysis allows controlling the SNR of each interval and, therefore, comparing the accuracy of each configuration versus the number of intervals.

Figure 2 compares the original chirp signal and both setups in time and frequency domains. The first column corresponds to Mode 1: *Constant Interval Energy*. For this setup, the value T was fixed to 100 μs and the energy to 5.2 mJ in each frequency interval. Therefore, the more intervals, the greater the total injected energy. In the frequency domain, it can be noticed that the total energy is four times (four intervals) greater than in the original chirp one.

The second column corresponds to Mode 2: "*Constant Total Energy*". In this configuration, the total energy injected was fixed to 5.2 mJ by reducing parameter T depending on the number of intervals. Its spectrum shows that the energy of each interval is reduced to keep constant the total energy (by keeping down the signal duration). Table 1 summarizes the main parameters of these setups for different number of intervals.

[2] $C(x)$ and $S(x)$ are the Fresnel integrals defined as $C(x) = \int_0^x cos(t^2)dt$ and $S(x) = \int_0^x sin(t^2)dt$.

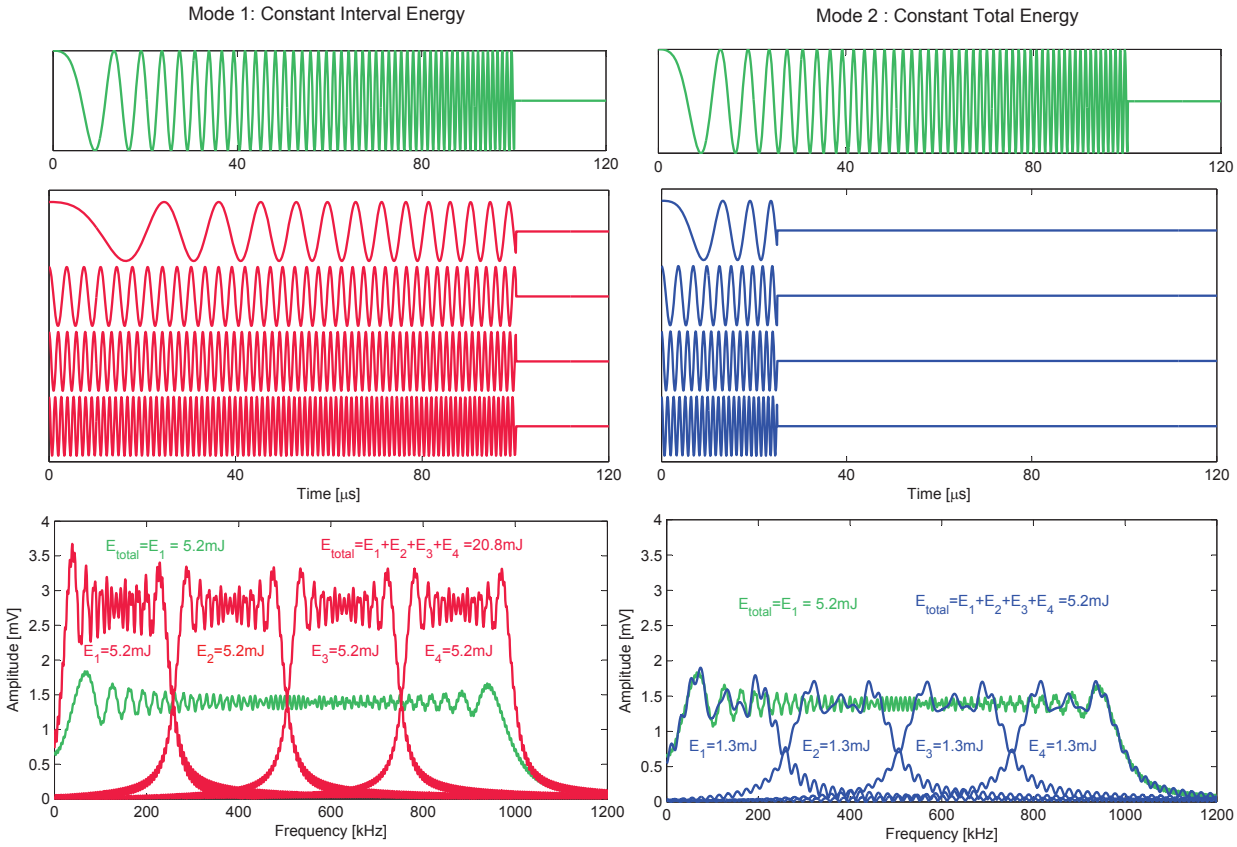

Figure 2: Comparison between a original chirp signal and its equivalent signals, Mode 1 (Constant Interval Energy) and Mode 2 (Constant Total Energy)in the time domain (second row) and frequency domain (third row).

Table 1: Main parameters of each configuration: Constant Interval Energy and Constant Total Energy.

Number of	Bandwidth/	Mode 1: Constant Interval Energy			Mode 2: Constant Total Energy		
intervals	int $[kHz]$	T/int $[\mu s]$	E/int $[mJ]$	E_{Tot} $[mJ]$	T/int $[\mu s]$	E/int $[mJ]$	E_{Tot} $[mJ]$
1	990	100	5.2	5.2	100	5.2	5.2
2	495	100	5.2	10.4	50	2.6	5.2
4	247.5	100	5.2	20.8	25	1.3	5.2
6	165	100	5.2	31.2	16.6	0.9	5.2
8	123.75	100	5.2	41.6	12.5	0.6	5.2
10	99	100	5.2	52	10	0.5	5.2

3. Experimental

3.1. Materials and sample preparation

Mortar specimens according to Spanish standard UNE EN 196-1:2005 [18] were manufactured. In order to improve the statistical analysis of the processed signals, three mixes were performed. Each mix is composed of 450 grams of CEM I 52,5-R Portland cement, 1350 grams of silica sand and 225 grams of water. The result of these mixes were nine specimens of 40x40x160 mm^3 standardized mortar, with 0.5 water to cement ratio

and 1:3 cement to aggregate ratio. After the iron moulds were filled with the fresh mortar, they were stored in wet chamber (20 °C and 100% RH) for 24 hours. After that, specimens were released and cured under water (saturated with calcium hydroxide) at 20 °C in the wet chamber for 90 days.

3.2. Test layout

An ultrasonic through-transmission setup was selected because it offers good penetration and good accuracy for attenuation determination. The disposition of the equipment is shown in Fig. 3. The transducers (transmitter and receiver) used were the $K1SC$ (General Electric). Both are broadband transducers with a bandwidth centered at 1 MHz.

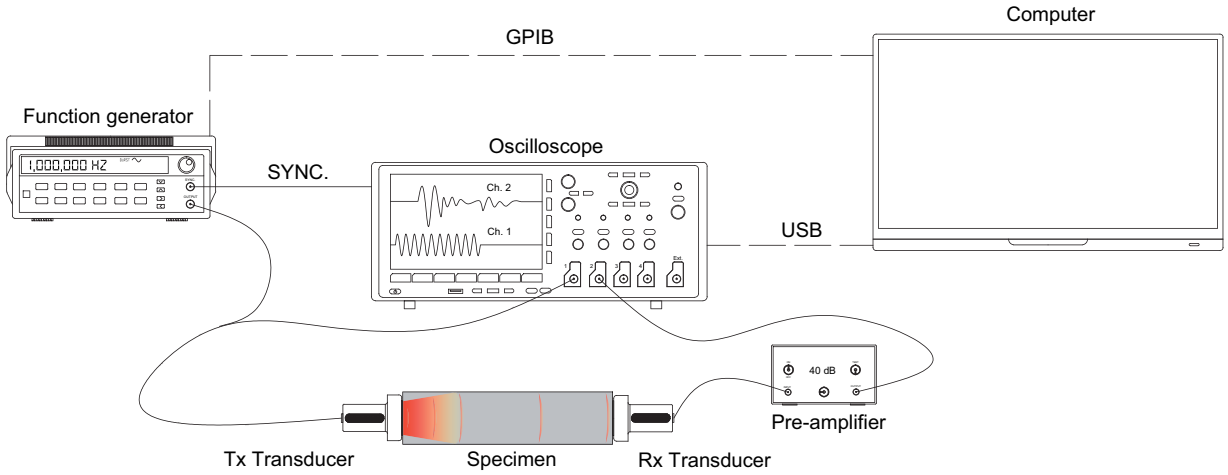

Figure 3: Scheme of equipment used in a typical ultrasonic inspection.

The transmitter transducer was excited directly by a programmable signal generator (Agilent 33120A) while the reception transducer was connected to a 40 dB preamplifier (Panametrics 5600B). The received and amplified ultrasonic signal was captured using a digital oscilloscope (Tektronix $DPO3014$) with a sampling frequency of 25 MHz. Finally, a laptop was used to control the signal generator and to acquire and store the digitized signals. The ultrasonic transducers were placed facing the longitudinal axis of the specimen. They were fixed by two plastic clamps: a movable one to adjust to the specimen, and a fixed one. Ultrasonic gel at the transducer specimen interface was used as an impedance coupling medium.

3.3. Calibration process

The calibration process was carried out with the emitter and receiver transducers face to face without any material between them. In this situation, Eq. (2) simplifies into Eq. (17) (due to the absence of the tested material):

$$\alpha_{equip}(f) = S_{tx}(f) - S_{rx}(f)\,[dB] \tag{17}$$

where $S_{tx}(f)\ [dB]$ is the energy spectral density (ESD) of the transmitted signal and $S_{rx}(f)\ [dB]$ is the ESD of the received signal. Both variables must be computed according to the analyzed expressions seen in Section 2, depending on the transmitted waveform. The testing process parameters were equal to the material analysis ones except for the transmitted signal amplitude which was reduced up to 0.5 Vp, to avoid saturation.

Figure 4 shows the $-\alpha_{equip}(f)$ obtained from calibration process. Three curves correspond to the three different transmitted signals: sinusoidal, burst and chirp signals. The fact that the curves are almost equivalent (mean standard deviation is 2.67%) reveals that outlined expressions in the Section 2 are correct. This curves are used to compensate the received signal during the material measurement process.

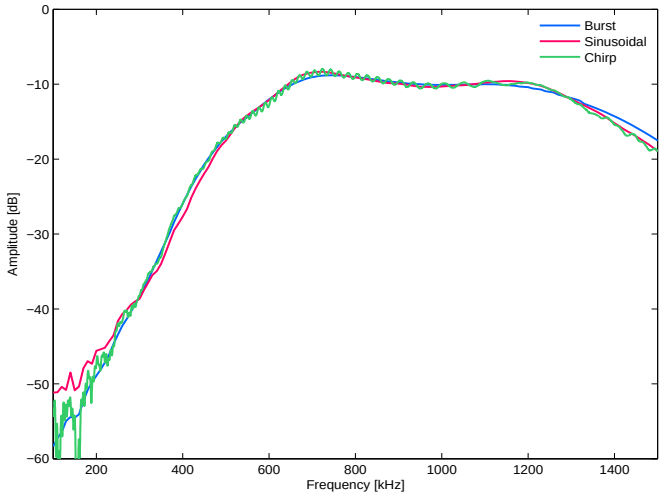

Figure 4: Frequency response of measurement equipment ($-\alpha_{equip}(f)$).

4. Results and discussion

In this section, the results for the three types of signals are presented. The common parameter for all the signals is the amplitude of the transmitted signal that was fixed to $A_{tx} = 10V$. For burst signal, the number of cycles was $N = 5$. For sinusoidal and burst signals, the signal generator was set to sweep the fundamental frequency, f_0, from 1 kHz up to 1 MHz with increments of $5kHz$ and a delay of 1 second between each analysed frequency. Therefore, for each specimen, 200 measurements were acquired (one for each fundamental frequency) and a frequency response of 200 points is obtained for α_{mat}. For chirp signal, the analysed bandwidth was the same to sinusoidal and burst signals, but with just one measurement. Next subsections describe and compare the results of the three signals applied to prismatic mortar specimens.

4.1. Sinusoidal signal

The attenuation curve, $\alpha_{mat}(f)$, obtained with a transmitted sinusoidal signal using the expressions raised in Section 2.1 is shown in Fig 5. It can be noticed the positive trend of the attenuation values as frequency increases, as well as its low dispersion between measures (the shadowed area represents the 90 % confidence intervals).

The evolution of the attenuation curve is proportional to the internal composition of the material under study (as frequency increases the attenuation parameter is sensitive to smaller particles/inhomogeneities). However, the results of attenuation obtained for frequencies below 450 kHz are likely to correspond to the propagation of surface waves, proportional to the mechanical properties of the material and its geometry and not so much to the internal composition.

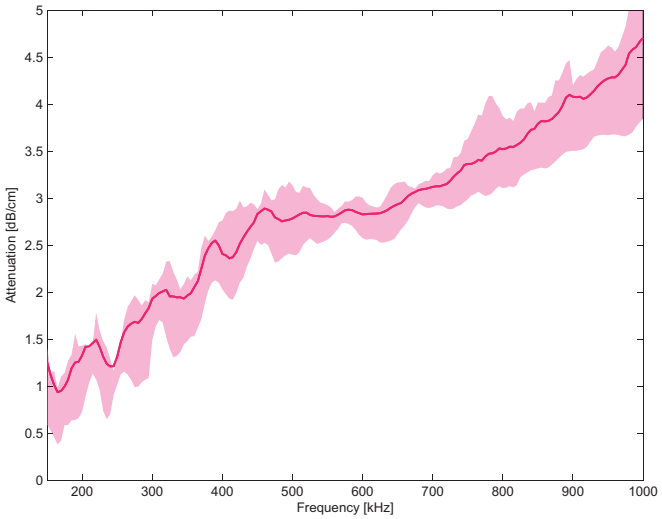

Figure 5: Frequency-dependent ultrasonic attenuation, $\alpha_{mat}(f)$, obtained with sinusoidal signal.

Along this Section, the attenuation curve obtained for sinusoidal input signal is defined as the reference attenuation curve. In order to compare the different obtained results, it will be computed the root-mean-square error ($error_{RMS}$) expressed as in Eq. 18, where the function $error(f)$ is defined as Eq. 19.

$$error_{RMS} = \sqrt{\frac{1}{f_2 - f_1}\int_{f_1}^{f_2} |error(f)|^2 df} \tag{18}$$

$$error(f) = \alpha(f) - \alpha_{reference}(f) \tag{19}$$

4.2. Burst signal

The attenuation obtained with the burst sinusoidal signal is shown in Fig. 6. The result has the same trend as the case of the pure sinusoidal signal but it seems to have an smoother behavior. It is due to the fact that the attenuation herein is computed as the integral of the power spectrum in the main lobe of the fundamental frequency (Eq. 11), which implies a frequency filtering. Fig. 7 compares the attenuation curves obtained with sinusoidal and burst signals. The $error_{RMS}$ between both curves is 0.15 dB (5.2%).

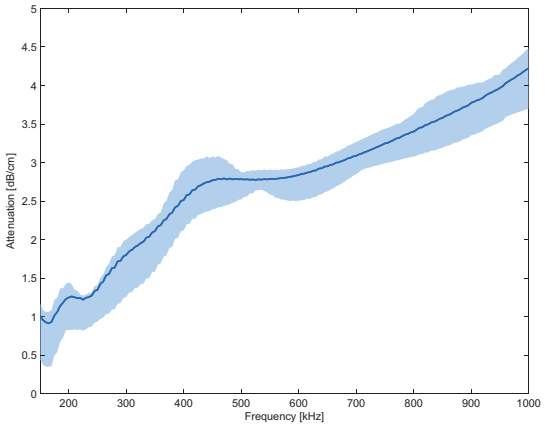

Figure 6: Frequency-dependent ultrasonic attenuation, $\alpha_{mat}(f)$, obtained with burst signal.

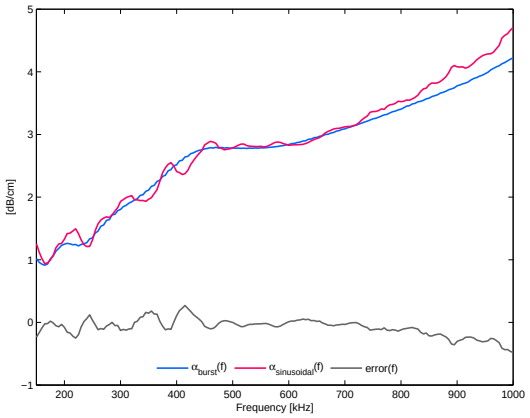

Figure 7: Comparison between the frequency-dependent ultrasonic attenuation, $\alpha_{mat}(f)$, obtained with sinusoidal (red) and burst (blue) signals. Error curve (black), $error(f)$ between both aforementioned results.

4.3. Chirp signal

In this section, the results obtained for chirp signal are presented. Firstly, both setups ("Constant Interval Energy" and "Constant Total Energy") are analyzed in terms of the $error_{RMS}$ and compared in order to determine the optimal setup. To join this aim, the total bandwidth has been divided in different number of frequency intervals, as it has been explained in Section 2.3. With the optimal setup, the results are offered and compared with sinusoidal and burst signals.

Table 2 shows the mean value of $error_{RMS}$ for the two setups and the different number of intervals. The error between them are quite similar although "Constant Interval Energy" is slightly lower than "Constant Total Energy" as the number of intervals increases. The error is smaller for Mode 1 and as the number of intervals increases seems logical since it enhances the injected energy for the analysis of the material. However, the differences between configurations are not very significant because the material do not attenuate too much and any setup allows enough SNR for the required analysis.

Table 2: RMS Error for intervals and setup mode

Number of intervals	Bandwidth per interval $[kHz]$	Mode 1: Constant Interval Energy $error_{RMS}$ [dB]	Mode 2: Constant Total Energy $error_{RMS}$ [dB]
1	990	0.22 ± 0.05	0.23 ± 0.04
2	495	0.21 ± 0.04	0.25 ± 0.04
4	247.5	0.22 ± 0.05	0.25 ± 0.03
6	165	0.20 ± 0.05	0.24 ± 0.04
8	123.75	0.21 ± 0.04	0.25 ± 0.02
10	99	0.20 ± 0.04	0.23 ± 0.03

Fig. 8 and 9 represent three curves: sinusoidal attenuation (as reference attenuation), chirp attenuation and $error(f)$ for "Constant Interval Energy" setup for one specimen. Fig. 8 corresponds to 1 interval (the bandwidth

is not divided), meanwhile Fig. 9 corresponds to 4 intervals. As it can be appreciated, both graphs offer similar trends and errors despite having been used four independent signals in the latter case.

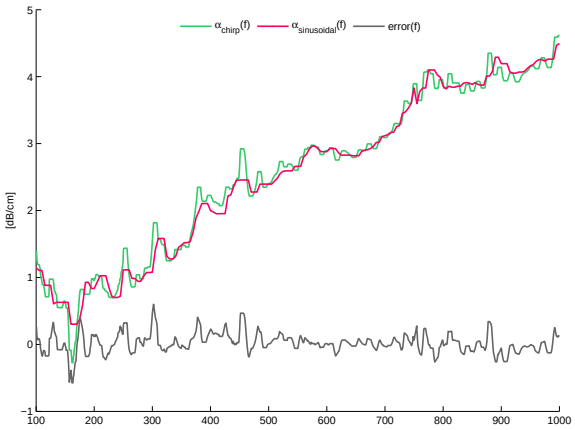

Figure 8: Comparison between the frequency-dependent ultrasonic attenuation, $\alpha_{mat}(f)$, obtained with sinusoidal (red) and original chirp (green) signals. Error curve (black), $error(f)$ between both aforementioned results.

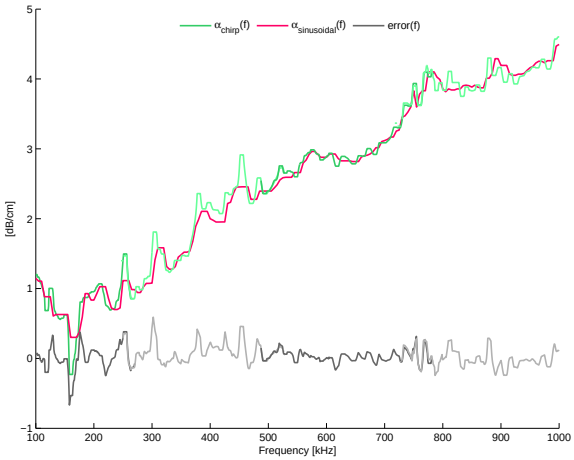

Figure 9: Comparison between the frequency-dependent ultrasonic attenuation, $\alpha_{mat}(f)$, obtained with sinusoidal signal (red) and original chirp signal (green) divided in four intervals (Mode 1). Error curve (black), $error(f)$ between both aforementioned results.

Taking into account that using the configuration "Constant Interval Energy" no significant improvement is achieved dividing the chirp signal in subintervals, only 1 interval is selected as optimal setup for attenuation estimation by means of the chirp signal. The attenuation obtained with chirp signal is shown in Fig. 10. Mean attenuation curves of the three analyzed signals are superimposed and showed in Fig. 11 to be compared. Similar behaviors can be appreciated for the three methods with minimal deviations. The behavior of chirp attenuation is more similar to sinusoidal attenuation because none of them perform a bandwidth integration for attenuation estimation as burst signal does. The $error_{RMS}$ (assuming sinusoidal curve as reference one) is 0.15 dB for burst signal and 0.08 dB for chirp signal, it means, the three signal offer similar estimations for $\alpha(f)$. Table 3 summarizes all the quantified results: the mean value of the deviation between measures, the $error_{RMS}$, as well as the acquisition time needed by each transmitted signal assuming that 200 points of the curve of attenuation are analyzed.

Table 3: Comparison of results between different transmitted signals. The acquisition time has been computed as the sum of the transmitted time (approximately 0.5 seconds) and the delay between measurements (1 second, enough the signal to stabilize).

	Deviation [dB]	$error_{RMS}$ [dB]	Acquisition time [s]
Sinusoidal signal	0.35	-	300
Burst signal	0.28	0.15	300
Chirp signal	0.34	0.08	0.5

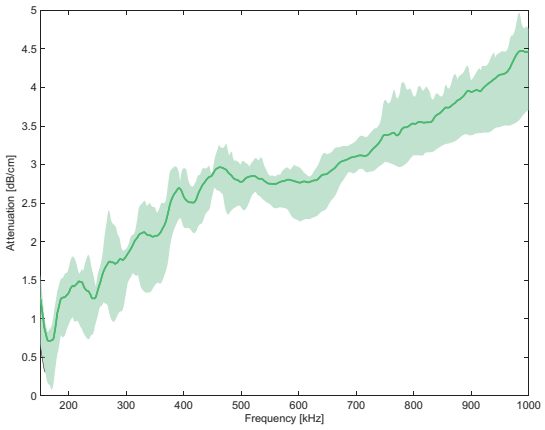

Figure 10: Frequency-dependent ultrasonic attenuation, $\alpha_{mat}(f)$, obtained with chirp signal.

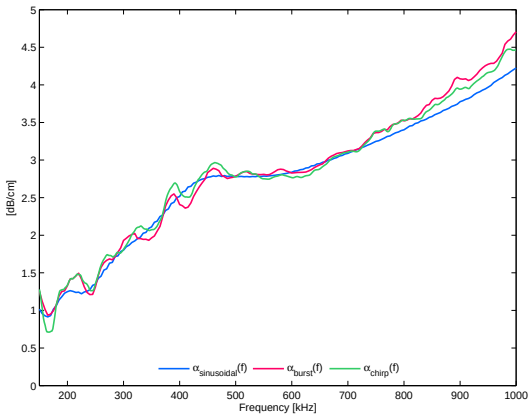

Figure 11: Comparison between the frequency-dependent ultrasonic attenuation, $\alpha_{mat}(f)$, obtained with sinusoidal (red), burst (blue) and chirp (green) signals.

5. Conclusions

In this paper the study of frequency-dependent ultrasonic attenuation in strongly heterogeneous materials was addressed. To determine the attenuation accurately over a wide frequency range, it is necessary to have suitable excitation techniques. In this study, three kinds of transmitted signals have been analyzed, grouped according to their bandwidth: narrowband and broadband signals. Its mathematical formulation has revealed the relationship between the distribution of energy in their spectra and its immunity to noise. Sinusoidal and burst signals present higher SNR but a large number of measurements to cover the frequency range is needed. However, the linear swept-frequency signals (chirp) at the expense of lower SNR improve the effective bandwidth covering a wide frequency range with a single measurement and equivalent accuracy. In the case of highly attenuating materials, it is proposed the use of different configurations of the chirp signals which enable to inject more energy, and therefore, to improve the sensitivity of the technique without involving a high time cost. So that, if the attenuation of material and the sensitivity of measurements equipment allow the use of broadband signals, the combination of this kind of signals and the suitable signal processing result in an optimal estimate of $\alpha(f)$ with a minimum measurement time. In future applications, the use of the optimal configuration for proper monitoring of processes with high temporal variation is proposed. Such processes do not allow the acquisition of a large number of measurements at a fixed fundamental frequency, and therefore, require the use of swifter techniques.

Aknowledgements

This work has been supported by Spanish Administration under grant BIA2014-55311-C2-2-P.

References

[1] P. Aïtcin, Binders for Durable and Sustainable Concrete, Modern Concrete Technology, Taylor & Francis, ISBN 9780415385886, 2007.

[2] N. C. V.M. Maholtra, Non destructive testing on concrete, CMC, 2003.
[3] X. G. Tang, Y. J. Xie, G. C. Long, Application of Non-Destructive Technology in Evaluating Concrete to Sulfate Attack, Advanced Materials Research 168-170 (2010) 2565–2570.
[4] K. J. Leśnicki, J.-Y. Kim, K. E. Kurtis, L. J. Jacobs, Characterization of ASR damage in concrete using nonlinear impact resonance acoustic spectroscopy technique, NDT & E International 44 (8) (2011) 721–727.
[5] C. Payan, V. Garnier, J. Moysan, P. a. Johnson, Applying nonlinear resonant ultrasound spectroscopy to improving thermal damage assessment in concrete, The Journal of the Acoustical Society of America 121 (4) (2007) EL125.
[6] M. Molero, I. Segura, S. Aparicio, M. G. Hernández, M. a. G. Izquierdo, On the measurement of frequency-dependent ultrasonic attenuation in strongly heterogeneous materials., Ultrasonics 50 (8) (2010) 824–8.
[7] M. Diallo, M. Prasad, E. Appel, Comparison between experimental results and theoretical predictions for P-wave velocity and attenuation at ultrasonic frequency, Wave Motion 37 (1) (2003) 1–16.
[8] D. Aggelis, T. Philippidis, Ultrasonic wave dispersion and attenuation in fresh mortar, NDT & E International 37 (8) (2004) 617–631.
[9] V. Garnier, B. Piwakowski, O. Abraham, G. Villain, C. Payan, J. F. Chaix, Acoustic techniques for concrete evaluation: Improvements, comparisons and consistency, Construction and Building Materials 43 (2013) 598–613.
[10] T. P. Philippidis, D. G. Aggelis, Experimental study of wave dispersion and attenuation in concrete., Ultrasonics 43 (7) (2005) 584–95.
[11] T. Seldis, Enhanced experimental approach to measure the absolute ultrasonic wave attenuation., Ultrasonics 50 (1) (2010) 9–12.
[12] P. Gaydecki, F. Burdekin, The propagation and attenuation of medium-frequency ultrasonic waves in concrete: a signal analytical approach, Measurement Science ... 126.
[13] A. A. Shah, Y. Ribakov, C. Zhang, Efficiency and sensitivity of linear and non-linear ultrasonics to identifying micro and macro-scale defects in concrete, Materials & Design 50 (2013) 905–916.
[14] B.-C. Kim, J.-Y. Kim, Characterization of ultrasonic properties of concrete, Mechanics Research Communications 36 (2) (2009) 207–214.
[15] W. Punurai, J. Jarzynski, J. Qu, K. E. Kurtis, L. J. Jacobs, Characterization of entrained air voids in cement paste with scattered ultrasound, NDT & E International 39 (6) (2006) 514–524.
[16] W. Punurai, J. Jarzynski, J. Qu, J.-Y. Kim, L. J. Jacobs, K. E. Kurtis, Characterization of multi-scale porosity in cement paste by advanced ultrasonic techniques, Cement and Concrete Research 37 (1) (2007) 38–46.
[17] S. Soliman, M. Srinath, Continuous and discrete signals and systems, Prentice-Hall information and system sciences series, Prentice Hall, ISBN 9780135184738, 1998.
[18] UNE, EN 196-1:2005. Métodos de ensayo de cementos. Parte 1: Determinación de resistencias mecánicas, 2005.